Title	Graphene perfect absorber based on degenerate critical coupling of toroidal mode
Author(s)	Xu, Rongyang; Fujikata, Junichi; Takahara, Junichi
Citation	Optics Letters. 2023, 48(6), p. 1490-1493
Version Type	AM
URL	https://hdl.handle.net/11094/91298
rights	© 2023 Optica Publishing Group. One print or electronic copy may be made for personal use only. Systematic reproduction and distribution, duplication of any material in this paper for a fee or for commercial purposes, or modifications of the content of this paper are prohibited.
Note	

Graphene perfect absorber based on degenerate critical coupling of toroidal mode

RONGYANG XU[1], JUNICHI FUJIKATA[2], AND JUNICHI TAKAHARA[1,3,*]

[1]*Graduate School of Engineering, Osaka University, 2-1 Yamadaoka, Suita, Osaka 565-0871, Japan*
[2]*Institute of Post-LED Photonics (pLED), Tokushima University, 2-1 Minami-Josanjima, Tokushima 770-8506, Japan*
[3]*Photonics Center, Graduate School of Engineering, Osaka University, 2-1 Yamadaoka, Suita, Osaka 565-0871, Japan*

**Corresponding author: takahara@ap.eng.osaka-u.ac.jp*

Received XX Month XXXX; revised XX Month, XXXX; accepted XX Month XXXX; posted XX Month XXXX (Doc. ID XXXXX); published XX Month XXXX

Graphene is a two-dimensional material with great potential for photodetection and light modulation applications owing to its high charge mobility. However, the light absorption of graphene in the near-infrared range is only 2.3%, limiting the sensitivity of graphene-based devices. In this study, we propose a graphene perfect absorber based on degenerate critical coupling comprising monolayer graphene and hollow silicon Mie resonator array. In particular, the monolayer graphene achieves perfect absorption by controlling the period and holes of the Mie resonators. The proposed graphene perfect absorber can significantly improve the sensitivity of graphene-based devices.

Graphene with ultra-high charge mobility [1] has great potential for applications in high-speed photodetection [2–4] and light modulation [5,6]. However, for normal incident light, the absorption of monolayer graphene is only 2.3% in the near-infrared (NIR) range [7] due to ultra-short interaction length, limiting the sensitivity of graphene-based devices. The absorption of graphene can be improved by placing it on plasmonic metasurfaces based on localized surface plasmon resonance [3,8]. In particular, plasmonic metasurfaces are subwavelength-thick thin films composed of artificial nanostructures. Moreover, the electric field near plasmonic metasurfaces is enhanced at resonance, improving the interaction between light and graphene. However, metals are lossy in the NIR range, and a significant fraction of the incident light is attenuated by plasmonic metasurfaces. Consequently, the absorption of the monolayer graphene is still limited (e.g., 10% [3]).

Dielectric metasurfaces made of lossless materials support Mie-type resonant modes, including electric dipole (ED), magnetic dipole (MD), and toroidal electric dipole (TED) modes [9–11]. By combining graphene with lossless dielectric metasurfaces, graphene has the potential to achieve perfect absorption because the lossless dielectric metasurfaces do not attenuate the incident light. However, for conventional Mie resonators, such as cylindrical, cubic, and spherical Mie resonators, the enhanced field at resonance is primarily confined to the interior of the Mie resonators [12]. Hence, these Mie resonators cannot achieve high absorption of graphene.

The absorption of graphene can be changed by modifying the geometry of Mie resonators to control the field distribution and radiative loss γ of the resonant modes [9]. The field distribution of the resonant modes is related to material loss δ because the absorption of graphene is enhanced when the enhanced field extends outside the Mie resonators and overlaps with graphene in space. Thus, by matching γ with δ (the condition of critical coupling), graphene placed on nanodisk Mie resonators based on magnetic dipole quasi-bound states in the continuum resonance achieves nearly 50% absorption [13]. In previous studies, perfect absorption of monolayer dielectric Mie resonators was achieved by degenerate critical coupling (DCC) of Mie-type resonant modes [14–17]. We hypothesize that this concept applies to combining graphene and dielectric Mie resonators.

In this study, we propose a graphene perfect absorber comprising graphene and hollow Mie resonators whose perfect absorption relies on the DCC of the TED and MD modes. We show that the γ of the TED mode can be tuned by changing the period of the Mie resonators. In addition, the hole in the Mie resonators provides an additional parameter to tune the peak wavelength of the TED mode.

Fig. 1 shows the cuboid Mie resonator used in this study with lengths l_x and l_y and height h. The cuboid is shaped to be suitable for exciting the TED mode because a strong coupling between resonators is required to excite the TED mode [18]. In particular, a cuboid Mie resonator array enables strong near-field coupling between the resonators. We can control the γ of the TED mode by varying the period of the cuboid Mie resonators (See Supporting Information S1 for a comparison between the cuboid and nanodisk Mie resonators). Fig. 1b shows the multipole resonant modes of the cuboid Mie resonator in air. The multipole decomposition relies on induced current density in a Cartesian coordinate, which can be obtained from electric field distribution [11]. After obtaining the electric field distribution of the Mie resonator using a commercial 3D electromagnetic simulator (Ansys Lumerical FDTD), we perform the multipole decomposition based on an open-source MATLAB multipole expansion script [19] (see Supporting Information S2). The results show that the cuboid Mie resonator supports ED, TED, and MD resonant modes. This study does not consider higher-order modes, such as electric quadrupole (EQ) and magnetic quadrupole (MQ) modes, because the optical response of the quadrupole modes cannot be tuned by changing the period of the Mie resonators [10]. The ED is located at approximately 2000 nm. The TED appears at wavelengths shorter than 1900 nm, and the MD dominates at 1900 nm. The TED moment in the Cartesian coordinate used in this study is the higher-order term of an ED moment in a Spherical coordinate system [11,19]. For Mie resonator arrays in this study, the ED and TED have only one peak in spectra; therefore, there is only one even mode in the DCC system. The linewidth of the peak can be adjusted by controlling the destructive interference between the ED and TED.

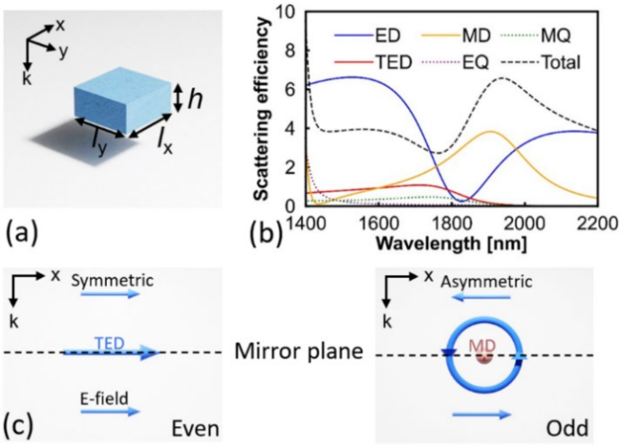

Fig. 1. (a) Schematic of a cuboid silicon Mie resonator in air. (b) Multipole decomposition of the silicon Mie resonator with $l_x = 672$ nm, $l_y = 700$ nm, and $h = 315$ nm. The incident electric field is polarized in the x-direction. Scattering efficiency is defined as the ratio of the scattering cross-section of the cuboid Mie resonator to its geometric cross-section. (c) Schematic of an even and an odd mode.

In this study, perfect absorption of graphene is achieved based on the DCC, which can be divided into the degenerate and critical coupling. For a mirror-symmetric system (e.g., a dielectric Mie resonator in air), an input beam from one port can be considered a combination of two pairs of counter-propagating beams with half the amplitude of the incident electric field. One pair of beams without phase difference can be coupled to even modes (e.g., TED mode). The other pair of beams with phase difference can be coupled to odd modes (e.g., MD mode). As shown in Fig. 1c, the TED is the even mode creating a symmetric electric field distribution in the forward and backward directions, while the MD is the odd mode creating an asymmetric electric field distribution. Owing to different symmetries, the even and odd modes are orthogonal and uncoupled [14,15]. Therefore, the two modes can be excited at the same wavelength (degenerate in wavelength). The absorption is a linear sum of the absorption of the even and odd modes. If γ of the even and odd modes matches δ, the modes are critically coupled and reach 50% absorption. We can achieve perfect absorption by satisfying the conditions of degenerate and critical coupling. Note that the wavelengths of the even and odd modes must be far from that of other higher-order modes to describe the behavior of the two modes with coupled-mode theory (CMT) [15]. The absorption equation based on the CMT is shown as follows [15]:

$$\boldsymbol{A} = \frac{2\gamma_1\delta_1}{(\omega-\omega_1)^2+(\gamma_1+\delta_1)^2} + \frac{2\gamma_2\delta_2}{(\omega-\omega_2)^2+(\gamma_2+\delta_2)^2}, \qquad (\mathbf{1})$$

where ω, ω_1, and ω_2 are the resonant frequencies of the incident light, TED, and MD modes, respectively, and γ_1, δ_1, γ_2, and δ_2 are the radiative and material losses of the TED and MD modes, respectively. According to Eq. 1, the absorption becomes unity at the resonance satisfying the degenerate ($\omega = \omega_1 = \omega_2$) and the critical coupling ($\gamma_1 = \delta_1$, $\gamma_2 = \delta_2$).

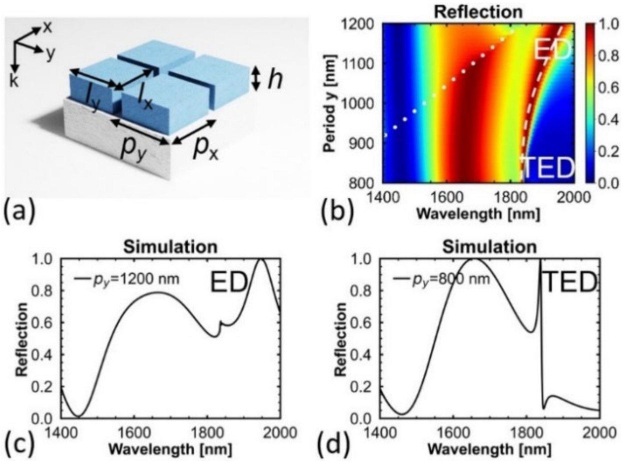

Fig. 2. (a) Schematic of a Mie resonator array without graphene. (b) Reflection spectral map of the Mie resonator array of $l_x = 672$ nm, $l_y = 700$ nm, $h = 315$ nm, $p_x = 810$ nm, and $p_y = 800–1200$ nm without graphene. The dotted line marks the wavelength of the Rayleigh anomaly. Reflection spectra at (c) $p_y = 1200$ nm and (d) $p_y = 800$ nm.

We study the collective response of Mie resonator arrays. Fig. 2a shows a schematic of the Mie resonator array used for the simulation (see Supporting Information S2 for the setting of the FDTD simulation). The crystalline silicon Mie resonators with period p_x and p_y are placed on a quartz substrate. The incident light is x-polarized. Therefore, the excited ED is along the x-direction. We note that the change in p_y significantly affects the peak linewidth of the ED mode, as shown in Fig. 2b. As p_y decreases, the peak linewidth of the ED mode also decreases. The white dotted line indicates the wavelength of the Rayleigh anomaly. Lattice resonances occur when the wavelength of the Rayleigh anomaly is close to that of the dipole modes [20,21]. However, the TED mode is excited by the arrays of the small periods; therefore, the wavelength of the Rayleigh anomaly is much smaller than that of the TED mode. Hence, we do not consider the Rayleigh anomaly. Fig. 2c shows the reflection spectrum of the Mie resonator array with $p_y = 1200$ nm. The reflection peak at 1945 nm is mainly due to the ED mode. To confirm the resonant mode, we plot the field distribution at 1945 nm in Fig. 3a, 3c, and 3e. Note that the ED induces a circular magnetic current loop. Moreover, the interaction between the Mie resonators in the y-direction is slightly strong. Hence, we can conclude that the ED mode dominates at 1945 nm.

As p_y decreases, the interaction of the Mie resonators in the y-direction is enhanced, and the TED mode is excited, which has a radiation pattern similar to that of the ED mode [11,18]. Fig. 2d shows the reflection spectrum at p_y = 800 nm. The reflection peak at 1838 nm exhibits a Fano-like spectral feature due to the interference of radiation fields between the ED and TED modes [22]. The destructive interference of the ED and TED modes can reduce γ. In particular, for a single Mie resonator, the destructive interference between the radiation of these two modes leads to a nonradiative mode, often referred to as an anapole [11,19,23]. Here, we call it the TED mode. To confirm the resonant mode, we plot the field distribution at 1838 nm in Fig. 3b, 3d, and 3f. Fig. 3f shows a strong interaction between the resonators in the y-direction with two electric poloidal current loops inside the resonator. Moreover, Fig. 3d shows the anti-parallel MDs induced by the electric poloidal current loops. Finally, the anti-parallel MDs induce the TED in Fig. 3b. These field distributions, especially the anti-parallel MDs in Fig. 3d, are representative characteristics of a low γ TED mode [18,22,24,25].

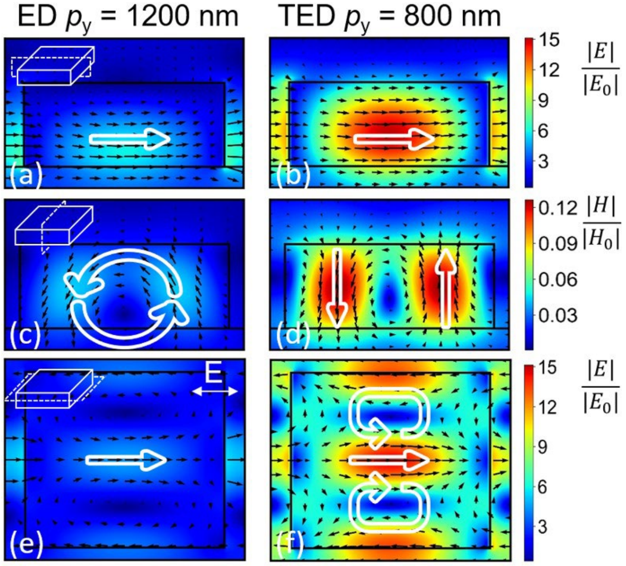

Fig. 3. Field distributions (total fields) of the Mie resonators with l_x = 672 nm, l_y = 700 nm, h = 315 nm, p_x = 810 nm, and p_y = 800 and 1200 nm. Electric field distribution for (a) p_y = 1200 nm at 1945 nm and (b) p_y = 800 nm at 1838 nm. Magnetic field distribution for (c) p_y = 1200 nm and (d) p_y = 800 nm. Top-view electric field distribution for (e) p_y = 1200 nm and (f) p_y = 800 nm.

Subsequently, monolayer graphene is put on the Mie resonator array, as shown in Fig. 4a. The monolayer graphene used in this simulation is from the build-in material database of Lumerical FDTD, which is based on the surface conductivity material model [26]. Fig. 4b shows the absorption spectral map of graphene absorbers with varying p_y. For p_y = 1200 nm, the absorption at 1943 nm is only 13.3% ($\gamma > \delta$). If the resonant mode is critically coupled ($\gamma = \delta$), absorption can be 50% [14,15]. As p_y decreases, γ of the resonant mode decreases and becomes close to δ. Hence, the absorption of graphene increases. At p_y = 800 nm, the absorption at 1840 nm is as high as 46.3% ($\gamma \approx \delta$) (see Supporting Information S3 for the effect of p_x). We present the optimization of the graphene absorber to achieve higher absorption in the following paragraphs.

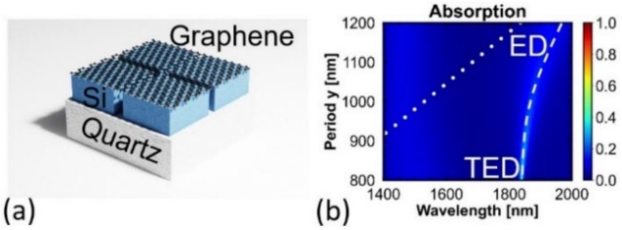

Fig. 4. (a) Schematic of the Mie resonator array with graphene. (b) Absorption spectral map of the Mie resonator arrays of l_x = 672 nm, l_y = 700 nm, h = 315 nm, p_x = 810 nm, and p_y = 800–1200 nm with monolayer graphene.

The TED and MD modes should degenerate in wavelength to achieve perfect absorption based on the DCC. In particular, we can use the hollow Mie resonators shown in Fig. 5a to adjust the peak wavelength of the TED mode. Fig. 5b shows the reflection spectral map of the Mie resonators with the different widths of hole w_x and w_y. As w_x and w_y increase, the peak wavelength of the TED mode has a larger blueshift than that of the MD mode. This is because the TED mode is associated with the collective polarization of the Mie resonator material. The effect of the appearance of holes is similar to that of reducing the length of the Mie resonators. Therefore, the peak wavelength of the TED mode is sensitive to the change in the w_x and w_y. However, the MD mode arises from a circular displacement current loop, the formation of which requires sufficient retardation of the incident electric field by the resonators. Hence, the peak wavelength of the MD mode is primarily affected by the h of the Mie resonators. Thus, by increasing the width of the holes, the peak wavelength of the TED mode can approach that of the MD mode. The two modes degenerate in wavelength at w_x = w_y = 210 nm.

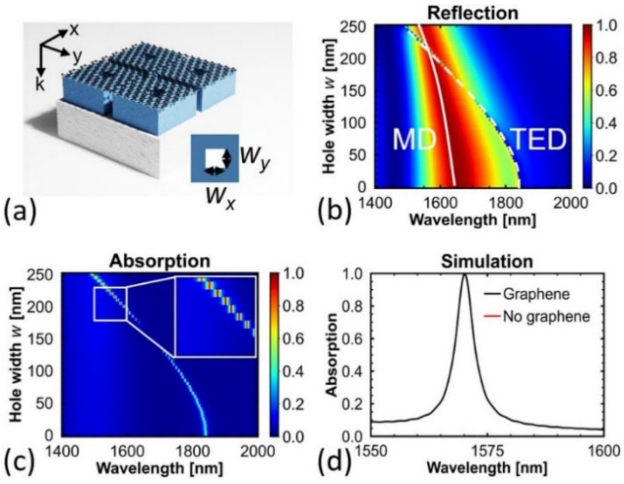

Fig. 5. (a) Schematic of the hollow Mie resonators with monolayer graphene. (b) Reflection and (c) absorption spectral maps of the hollow Mie resonators with l_x = 672 nm, l_y = 700 nm, w_x = w_y = 0–250 nm, h = 315 nm, p_x = 810 nm, and p_y = 800 nm. (d) Absorption spectra of the hollow Mie resonators of w_x = w_y = 210 nm with and without graphene.

Fig. 5c shows the absorption spectral map of the graphene absorbers with different w_x and w_y. For $w_x = w_y = 0$ nm, the absorption of graphene at 1840 nm is 46.3%. The absorption of graphene increases slightly with increasing w_x and w_y, increasing to 56% at $w_x = w_y = 100$ nm. This result is because the γ approaches δ as w_x and w_y change. However, if w_x and w_y increase further, the absorption of graphene almost disappears. The absorption is only 5% at $w_x = w_y = 160$ nm. This is because the nearly complete destructive interference of the TED and ED modes leads to a non-radiative TED mode, and the excitation of the TED mode from the far field is strongly suppressed. With increasing w_x and w_y, the complete destructive interference is not satisfied. At $w_x = w_y = 210$ nm, the TED mode achieves critical coupling and the TED and MD modes degenerate in wavelength. Hence, the graphene achieves perfect absorption, as shown in Fig. 5d. If we remove the graphene, the absorption of the hollow Mie resonators is close to 0 since silicon is lossless in the NIR region. Hence, the monolayer graphene absorbs more than 99.6% of the incident light at 1570 nm. We note that the Q-factor of the absorption peak at 1570 nm is approximately 340, implying a photon lifetime of at least a few hundred femtoseconds (fs) in the hollow Mie resonators (see Supporting Information S4 for variation of the electric field with time). The photon lifetime in the hollow Mie resonators is longer than the graphene carrier relaxation time dominated by intraband carrier-carrier scattering, demonstrated to be less than 10 fs [27]. The ultrafast relaxation allows graphene to absorb light continuously.

Finally, we study the angle-dependent absorption of the proposed graphene perfect absorber. For p-polarized incident light, the perfect absorber achieves 80% absorption at an incident angle of 8° (see Supporting Information S5). The absorption of the perfect absorber decreases with increasing incident angle. This is because the peak wavelength of the MD mode is angle-dependent [10,20]. At an incident angle greater than 8°, the TED and MD modes are not degenerate in wavelength. For s-polarized incident light, the absorption of the graphene is greater than 80% at an incident angle of 14° (see Supporting Information S5).

In conclusion, we proposed a graphene perfect absorber based on the DCC that comprises hollow silicon Mie resonators and monolayer graphene (see Supporting Information S6 for comparing absorbers). We tuned the γ of the TED mode by varying the period of the Mie resonators. The hole of the hollow Mie resonators introduces an additional parameter to adjust the peak wavelength of the TED mode. Thus, by changing the period and the hole of the Mie resonators, the monolayer graphene can achieve perfect absorption (99.6%) based on the DCC. Surprisingly, the sensitivity to the incident angle of light of the proposed perfect absorption is minimal. For p-polarized light with an incident angle of 8°, the absorption of graphene exceeds 80 %. For s-polarized light, the graphene perfect absorber can absorb 82% of the incident light at an incident angle of 14°. The proposed graphene perfect absorber has great potential in light modulation, sensing, and photodetection applications. In addition to graphene, we believe that the concept of the DCC-based perfect absorber can also apply to other lossy 2D materials. Hence, our study also provides an excellent platform for enhancing light-matter interactions in 2D materials.

Funding. Japan Society for the Promotion of Science (JSPS) KAKENHI (Grant No. JP22K18987 and No. JP22H01555); Research grant by Support Center for Advanced Telecommunications Technology Research (SCAT).

Disclosures. The authors declare no conflicts of interest.

Data availability. Data underlying the results presented in this paper are not publicly available at this time but may be obtained from the authors upon reasonable request.

Supplemental document. See Supplement 1 for supporting content.

References

1. K. I. Bolotin, K. J. Sikes, Z. Jiang, M. Klima, G. Fudenberg, J. Hone, P. Kim, and H. L. Stormer, Solid State Commun. **146**, 351 (2008).
2. A. Rogalski, Adv. Opt. Photon. **11**, 314 (2019).
3. Y. Yao, R. Shankar, P. Rauter, Y. Song, J. Kong, M. Loncar, and F. Capasso, Nano Lett. **14**, 3749 (2014).
4. X. Gan, R.-J. Shiue, Y. Gao, I. Meric, T. F. Heinz, K. Shepard, J. Hone, S. Assefa, and D. Englund, Nature Photon **7**, 883 (2013).
5. G. Kovacevic, C. Phare, S. Y. Set, M. Lipson, and S. Yamashita, Appl. Phys. Express **11**, 065102 (2018).
6. M. Liu, X. Yin, E. Ulin-Avila, B. Geng, T. Zentgraf, L. Ju, F. Wang, and X. Zhang, Nature **474**, 64 (2011).
7. K. F. Mak, M. Y. Sfeir, Y. Wu, C. H. Lui, J. A. Misewich, and T. F. Heinz, Phys. Rev. Lett. **101**, 196405 (2008).
8. Y. Liu, W. Huang, T. Gong, Y. Su, H. Zhang, Y. He, Z. Liu, and B. Yu, Nanoscale **9**, 17459 (2017).
9. R. Xu and J. Takahara, Appl. Phys. Lett. **120**, 201104 (2022).
10. R. Xu and J. Takahara, Appl. Phys. Express **15**, 122003 (2022).
11. A. E. Miroshnichenko, A. B. Evlyukhin, Y. F. Yu, R. M. Bakker, A. Chipouline, A. I. Kuznetsov, B. Luk'yanchuk, B. N. Chichkov, and Y. S. Kivshar, Nat. Commun. **6**, 8069 (2015).
12. N. Bosio, H. Šípová-Jungová, N. O. Länk, T. J. Antosiewicz, R. Verre, and M. Käll, ACS Photonics **6**, 1556 (2019).
13. X. Wang, J. Duan, W. Chen, C. Zhou, T. Liu, and S. Xiao, Phys. Rev. B **102**, 155432 (2020).
14. J. R. Piper, V. Liu, and S. Fan, Appl. Phys. Lett. **104**, 251110 (2014).
15. X. Ming, X. Liu, L. Sun, and W. J. Padilla, Opt. Express **25**, 24658 (2017).
16. R. Xu and J. Takahara, Opt. Lett. **46**, 805 (2021).
17. R. Xu and J. Takahara, Opt. Lett. **46**, 3596 (2021).
18. J. Jeong, M. D. Goldflam, S. Campione, J. L. Briscoe, P. P. Vabishchevich, J. Nogan, M. B. Sinclair, T. S. Luk, and I. Brener, ACS Photonics **7**, 1699 (2020).
19. T. Hinamoto and M. Fujii, OSA Continuum **4**, 1640 (2021).
20. V. E. Babicheva, MRS Commun. **8**, 1455 (2018).
21. D. Khlopin, F. Laux, W. P. Wardley, J. Martin, G. A. Wurtz, J. Plain, N. Bonod, A. V. Zayats, W. Dickson, and D. Gérard, J. Opt. Soc. Am. B **34**, 691 (2017).
22. S.-D. Liu, Z.-X. Wang, W.-J. Wang, J.-D. Chen, and Z.-H. Chen, Opt. Express **25**, 22375 (2017).
23. G. Grinblat, Y. Li, M. P. Nielsen, R. F. Oulton, and S. A. Maier, Nano Lett. **16**, 4635 (2016).
24. C. Cui, S. Yuan, X. Qiu, L. Zhu, Y. Wang, Y. Li, J. Song, Q. Huang, C. Zeng, and J. Xia, Nanoscale **11**, 14446 (2019).
25. J. F. Algorri, D. C. Zografopoulos, A. Ferraro, B. García-Cámara, R. Beccherelli, and J. M. Sánchez-Pena, Opt. Express **27**, 6320 (2019).
26. G. W. Hanson, J. Appl. Phys. **103**, 064302 (2008).
27. G. Xing, H. Guo, X. Zhang, T. C. Sum, and C. H. A. Huan, Opt. Express **18**, 4564 (2010).

1. K. I. Bolotin, K. J. Sikes, Z. Jiang, M. Klima, G. Fudenberg, J. Hone, P. Kim, and H. L. Stormer, "Ultrahigh electron mobility in suspended graphene," Solid State Commun. 146(9–10), 351–355 (2008).
2. A. Rogalski, "Graphene-based materials in the infrared and terahertz detector families: a tutorial," Adv. Opt. Photon. 11(2), 314 (2019).
3. Y. Yao, R. Shankar, P. Rauter, Y. Song, J. Kong, M. Loncar, and F. Capasso, "High-Responsivity Mid-Infrared Graphene Detectors with Antenna-Enhanced Photocarrier Generation and Collection," Nano Lett. 14(7), 3749–3754 (2014).
4. X. Gan, R.-J. Shiue, Y. Gao, I. Meric, T. F. Heinz, K. Shepard, J. Hone, S. Assefa, and D. Englund, "Chip-integrated ultrafast graphene photodetector with high responsivity," Nature Photon 7(11), 883–887 (2013).
5. G. Kovacevic, C. Phare, S. Y. Set, M. Lipson, and S. Yamashita, "Ultra-high-speed graphene optical modulator design based on tight field confinement in a slot waveguide," Appl. Phys. Express 11(6), 065102 (2018).
6. M. Liu, X. Yin, E. Ulin-Avila, B. Geng, T. Zentgraf, L. Ju, F. Wang, and X. Zhang, "A graphene-based broadband optical modulator," Nature 474(7349), 64–67 (2011).
7. K. F. Mak, M. Y. Sfeir, Y. Wu, C. H. Lui, J. A. Misewich, and T. F. Heinz, "Measurement of the Optical Conductivity of Graphene," Phys. Rev. Lett. 101(19), 196405 (2008).
8. Y. Liu, W. Huang, T. Gong, Y. Su, H. Zhang, Y. He, Z. Liu, and B. Yu, "Ultra-sensitive near-infrared graphene photodetectors with nanopillar antennas," Nanoscale 9(44), 17459–17464 (2017).
9. R. Xu and J. Takahara, "Highly sensitive and robust refractometric sensing by magnetic dipole of Si nanodisks," Appl. Phys. Lett. 120(20), 201104 (2022).
10. R. Xu and J. Takahara, "Angle-insensitive Huygens' metasurfaces of quadrupole modes," Appl. Phys. Express 15(12), 122003 (2022).
11. A. E. Miroshnichenko, A. B. Evlyukhin, Y. F. Yu, R. M. Bakker, A. Chipouline, A. I. Kuznetsov, B. Luk'yanchuk, B. N. Chichkov, and Y. S. Kivshar, "Nonradiating anapole modes in dielectric nanoparticles," Nat. Commun. 6(1), 8069 (2015).
12. N. Bosio, H. Šípová-Jungová, N. O. Länk, T. J. Antosiewicz, R. Verre, and M. Käll, "Plasmonic versus All-Dielectric Nanoantennas for Refractometric Sensing: A Direct Comparison," ACS Photonics 6(6), 1556–1564 (2019).
13. X. Wang, J. Duan, W. Chen, C. Zhou, T. Liu, and S. Xiao, "Controlling light absorption of graphene at critical coupling through magnetic dipole quasi-bound states in the continuum resonance," Phys. Rev. B 102(15), 155432 (2020).
14. J. R. Piper, V. Liu, and S. Fan, "Total absorption by degenerate critical coupling," Appl. Phys. Lett. 104(25), 251110 (2014).
15. X. Ming, X. Liu, L. Sun, and W. J. Padilla, "Degenerate critical coupling in all-dielectric metasurface absorbers," Opt. Express 25(20), 24658–24669 (2017).
16. R. Xu and J. Takahara, "Radiative loss control of an embedded silicon perfect absorber in the visible region," Opt. Lett. 46(4), 805–808 (2021).
17. R. Xu and J. Takahara, "All-dielectric perfect absorber based on quadrupole modes," Opt. Lett. 46(15), 3596 (2021).
18. J. Jeong, M. D. Goldflam, S. Campione, J. L. Briscoe, P. P. Vabishchevich, J. Nogan, M. B. Sinclair, T. S. Luk, and I. Brener, "High Quality Factor Toroidal Resonances in Dielectric Metasurfaces," ACS Photonics 7(7), 1699–1707 (2020).
19. T. Hinamoto and M. Fujii, "MENP: an open-source MATLAB implementation of multipole expansion for nanophotonics," OSA Continuum 4(5), 1640 (2021).
20. V. E. Babicheva, "Lattice effect in Mie-resonant dielectric nanoparticle array under oblique light incidence," MRS Commun. 8(04), 1455–1462 (2018).
21. D. Khlopin, F. Laux, W. P. Wardley, J. Martin, G. A. Wurtz, J. Plain, N. Bonod, A. V. Zayats, W. Dickson, and D. Gérard, "Lattice modes and plasmonic linewidth engineering in gold and aluminum nanoparticle arrays," J. Opt. Soc. Am. B 34(3), 691 (2017).
22. S.-D. Liu, Z.-X. Wang, W.-J. Wang, J.-D. Chen, and Z.-H. Chen, "High Q-factor with the excitation of anapole modes in dielectric split nanodisk arrays," Opt. Express 25(19), 22375 (2017).
23. G. Grinblat, Y. Li, M. P. Nielsen, R. F. Oulton, and S. A. Maier, "Enhanced Third Harmonic Generation in Single Germanium Nanodisks Excited at the Anapole Mode," Nano Lett. 16(7), 4635–4640 (2016).
24. C. Cui, S. Yuan, X. Qiu, L. Zhu, Y. Wang, Y. Li, J. Song, Q. Huang, C. Zeng, and J. Xia, "Light emission driven by magnetic and electric toroidal dipole resonances in a silicon metasurface," Nanoscale 11(30), 14446–14454 (2019).
25. J. F. Algorri, D. C. Zografopoulos, A. Ferraro, B. García-Cámara, R. Beccherelli, and J. M. Sánchez-Pena, "Ultrahigh-quality factor resonant dielectric metasurfaces based on hollow nanocuboids," Opt. Express 27(5), 6320 (2019).
26. G. W. Hanson, "Dyadic Green's functions and guided surface waves for a surface conductivity model of graphene," J. Appl. Phys. 103(6), 064302 (2008).
27. G. Xing, H. Guo, X. Zhang, T. C. Sum, and C. H. A. Huan, "The Physics of ultrafast saturable absorption in graphene," Opt. Express 18(5), 4564 (2010).